Dimerization Energetics of the G-protein Coupled Bile Acid Receptor TGR5 from All-atom Simulations

Lucas Wäschenbach[1], Christoph G. W. Gertzen[1,2,3], Verena Keitel[2], Holger Gohlke[1,3*]

[1] Institute for Pharmaceutical and Medicinal Chemistry, Heinrich Heine University Düsseldorf, 40225 Düsseldorf, Germany.

[2] Clinic for Gastroenterology, Hepatology and Infectious Diseases, Heinrich Heine University Düsseldorf, 40225 Düsseldorf, Germany.

[3] John von Neumann Institute for Computing (NIC), Jülich Supercomputing Centre (JSC), and Institute for Complex Systems - Structural Biochemistry (ICS-6), Forschungszentrum Jülich GmbH, 52425 Jülich, Germany.

Keywords: receptor oligomerization, membrane, signaling, potential of mean force, molecular dynamics simulations, MM-PBSA

[*]Address: Universitätsstr. 1, 40225 Düsseldorf, Germany.
Phone: (+49) 211 81 13662; Fax: (+49) 211 81 13847
E-mail: gohlke@uni-duesseldorf.de.

Abstract

We describe the first extensive energetic evaluation of GPCR dimerization on the atomistic level by means of potential of mean force (PMF) computations and implicit solvent/implicit membrane end-point free energy calculations (MM-PBSA approach). Free energies of association computed from the PMFs show that the formation of both the 1/8 and 4/5 interface is energetically favorable for TGR5, the first GPCR known to be activated by hydrophobic bile acids and neurosteroids. Furthermore, formation of the 1/8 interface is favored over that of the 4/5 interface. Both results are in line with our previous FRET experiments in live cells. Differences in lipid-protein interactions are identified to contribute to the observed differences in free energies of association. A per-residue decomposition of the MM-PBSA effective binding energy reveals hot spot residues specific for both interfaces that form clusters. This knowledge may be used to guide the design of dimerization inhibitors or perform mutational studies to explore physiological consequences of distorted TGR5 association. Finally, we characterized the role of Y111, located in the conserved (D/E)RY motif, as a facilitator of TGR5 interactions. The types of computations performed here should be transferable to other transmembrane proteins that form dimers or higher oligomers as long as good structural models of the dimeric or oligomeric states are available. Such computations may help to overcome current restrictions due to an imperfect energetic representation of protein association at the coarse-grained level.

Introduction

Knowledge of the dimerization interfaces of G-protein coupled receptors (GPCRs) can be exploited to modulate their signaling behavior with small molecules targeting those interfaces. Here, we present an energetic evaluation of dimerization of the GPCR TGR5. TGR5 is the first GPCR known to be activated by hydrophobic bile acids and neurosteroids, such as taurolithocholic acid (TLC) and pregnanediol, respectively.[1-6] Due to its role in various physiological functions, TGR5 is a target for the treatment of type II diabetes and metabolic syndrome, where TGR5 agonists may be beneficial. Furthermore, inhibition of TGR5 signaling may prove useful in cholangiocarcinoma, esophageal and gastric adenocarcinoma, and bile acid-induced itch.[7-14] The development of TGR5 antagonists is, hence, key to combat TGR5-associated types of cancer and itch in cholestatic liver diseases.[15]

Especially in the latter case ligands with a low side-effect profile are of utmost importance. Specifically targeting GPCR homodimers with bivalent ligands has been shown to reduce side effects on other GPCRs.[16,17] GPCR dimerization also has an influence on the trafficking from the endoplasmic reticulum to the plasma membrane, internalization, degradation, activation, and signaling, although the mechanisms are not completely understood.[16,18-23] Specifically disrupting the dimerization via peptides or small molecules can be a powerful tool to investigate the influences of GPCR dimerization or enable a new way to pharmacologically target GPCRs.[21]

We recently showed that TGR5 forms higher order oligomers, with interactions between the respective transmembrane helices 1 (TM1) and helices 8 (1/8 interface) as the primary dimerization interface.[24] The substitution Y111A$^{3.51}$ (position 3.51 denoted in the Ballesteros-Weinstein nomenclature[25] according to the GPCR database[26]), although not impacting dimerization via the 1/8 interface, abolishes oligomerization presumably occurring via TMs 4 and 5 (4/5 interface) or

TMs 5 and 6 (5/6 interface), which act as secondary dimerization interfaces (**Figure 1**).[24] All three types of interfaces have been observed in crystal structures of other GPCRs.[28-30] However, the exact nature of TGR5's secondary interface remains elusive.[24]

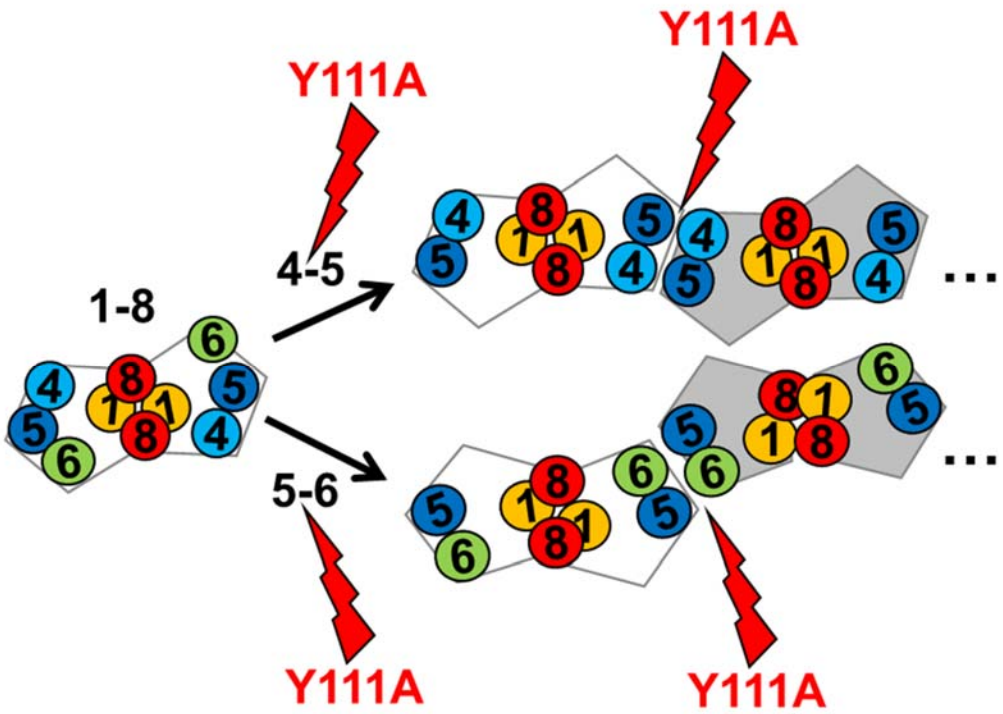

Figure 1. Schematic of TGR5 oligomerization. TGR5 protomers are represented as pentagons, transmembrane helices are represented as colored circles. The interference of the Y111A substitution with oligomerization is represented as red lightning bolts. In live cells, TGR5 forms dimers via the 1/8 interface, even in the presence of the Y111A substitution.[24] TGR5 also forms higher-order oligomers, likely dimers of dimers, with 1/8 as the primary dimerization interface and 4/5 or 5/6 as the secondary dimerization interface.[24] Formation of higher-order oligomers via interface 4/5 or 5/6 is abolished in the Y111A variant.[24] Figure was adapted from ref.[24]

Here, to further characterize the TGR5 dimerization interfaces, understand pathways of TGR5 dimerization, and the role of the Y111A$^{3.51}$ substitution in oligomer formation, we present an energetic evaluation of TGR5 dimerization. We computed potentials of mean force (PMF) applying umbrella sampling in the context of all-atom molecular dynamics (MD) simulations in an explicit solvent / explicit membrane environment to analyze the dimerization pathways of TGR5. Similar studies have been conducted on different GPCRs utilizing coarse-grained instead of all-atom

simulations and applying either PMF computations[31-33] or meta-dynamics approaches.[34] Yet, despite recent advances in the development of coarse-grained force fields[35-38] and in the coarse-grained representation of protein-lipid interactions,[39,40] the proper energetic representation of protein association at the coarse-grained level is still debated.[41,42] From the PMF of dimerization, we computed binding free energies[43] and equilibrium association constants using a scheme applied to coarse-grained simulations of GPCR dimerization.[33,44] This approach has also been applied to study small-molecule binding to proteins.[45,46]

Furthermore, employing dimer configurations from unbiased MD simulations started from structures located in the respective global minima of the free energy profiles, implicit membrane molecular mechanics Poisson-Boltzmann surface area (MM-PBSA) computations were performed to identify hot spot regions in the interfaces via per-residue decomposition of the effective binding energies. Together, these results represent the first extensive energetic evaluation of GPCR dimerization on the atomistic level and provide the structural foundation for developing small-molecule inhibitors of or performing mutational analyses on TGR5 dimerization.

Methods

Dimer models

To create TGR5 dimer models, initially, a homology model of the TGR5 protomer in the active conformation was generated because previous results[24] showed that the addition of an agonist had no influence on the di- or oligomerization of TGR5. In particular, no change in the distribution of Förster Resonance Energy Transfer (FRET) efficiencies was observed for TGR5 molecules tagged with fluorescent proteins at the C-termini,[24] so that it is safe to assume that the orientation of TGR5 molecules in a dimer does not change if the active state is adopted by TGR5. In turn, this finding excludes that TGR5 can adopt a dimer configuration in which a pronounced reorientation is necessary to adapt conformational changes upon activation. As particularly the intracellular end of transmembrane helix 6 (TM6) moves outwards upon GPCR activation,[47,48] we performed the subsequent simulations starting from TGR5 molecules in the active state to take into consideration a potential influence of TM6 movements on interface formation and energetics. The adoption of the inactive state from the active state takes about 6 μs.[49] As this is ~30-times longer than any of our individual simulations, TGR5 is expected to stay in the active state.

The active state model is based on the model of the inactive form of TGR5 generated previously by us[5] and the active state structure of the β_2-adrenergic receptor (PDB ID 3SN6[47]). For generating the model, TMs 1-4 and 7 and the extracellular parts of TMs 5 and 6 (residues 176-195 and 218-233, respectively), including the binding site, of the previous TGR5 model were used as template in a multiple sequence alignment, whereas for the intracellular parts of TMs 5 and 6 PDB ID 3SN6 was used. MODELLER 9.15[50] was then used to generate the active state model. The dimer models were subsequently created by aligning two TGR5 models onto the X-ray structures of GPCR dimers (PDB IDs 4DJH,[28] 3ODU,[29] and 4DKL[30]) that have 1/8, 4/5, and 5/6 interfaces,

respectively. While no structural clashes were present in the TGR5 dimer models with 1/8 and 4/5 interfaces, the intracellular parts of TMs 5 and 6 overlapped in the model with 5/6 interface. Note that the 5/6 interface was identified in a μ-opioid receptor dimer structure, where stabilizing mutations and an antagonist were present, preventing the adoption of an active state conformation.[30] In turn, the homologous [30] δ-opioid receptor monomerizes upon activation by morphine.[51] Thus, it seems safe to assume that the μ-opioid receptor dimer structure will also get distorted upon activation. Along these lines, preliminary modeling results of us indicate that, to resolve the clashes in the TGR5 dimer with 5/6 interface, the protomers would need to be separated by ~15 Å, resulting in a contact area of just four residues on each protomer, which should impact dimerization efficiency. Yet, no agonist-dependent effects on TGR5 dimerization were observed experimentally (see above).[24] Hence, we omitted the TGR5 dimer with 5/6 interface from further analyses.

Setup of simulation systems

The orientation of the dimers in the membrane was determined with the OPM webserver.[52] For each of the windows of the umbrella sampling simulations, a separate system was built. The membrane builder tool available on the CHARMM-GUI website[53] was used for embedding the dimers in a pre-equilibrated bilayer of DOPC lipids[54] using the replacement method.[55] The required rectangular simulation box was generated with water layers of 12 Å thickness above and below the protein. The total system size of the largest of these systems is ~140,000 atoms, including TIP3P water molecules[56] and 0.15 M KCl. The disulfide bridge between CYS 86 and 156 was included in the final models, and each protomer was capped with N-terminal acetyl (ACE) and C-terminal N-methyl amide (NME) moieties.

Molecular dynamics simulations

All MD simulations were performed using the AMBER 14 suite of programs,[57] with the ff14SB force field for the proteins,[58] the Lipid14 force field for the lipids,[59] the TIP3P water model,[56] and the Joung-Cheatham parameters for K and Cl ions.[60,61] The particle mesh Ewald method[62] was used to treat long-range electrostatic interactions, and bond lengths involving bonds to hydrogen atoms were constrained using the SHAKE algorithm.[63] The time step for integrating Newton's equations of motion was 2 fs with a direct-space, non-bonded cutoff of 10 Å. In the first step of minimization, 250 cycles of steepest descent were followed by conjugate gradient minimization for a total of 2000 cycles. Solute atoms were restrained by harmonic potentials with force constants of 500 kcal mol^{-1} $Å^{-2}$. In the second step, the force constants of the restraining potentials were decreased to 10 kcal mol^{-1} $Å^{-2}$, and 2500 cycles of steepest descent minimization followed by up to 10.000 cycles with the conjugate gradient method were performed. For thermalization, during 20 ps of NVT simulation, the system was heated to a temperature of 100 K using Langevin dynamics with a coupling constant of 1 ps^{-1} for temperature regulation. Heating to 303 K was carried out under NPT conditions using a Berendsen barostat with anisotropic pressure scaling and a reference pressure of 1 bar for 100 ps. Another 2.8 ns with harmonic restraints with a force constant of 10 kcal mol^{-1} $Å^{-2}$ followed.

The production runs were carried out with the GPU-accelerated version of PMEMD[64] applying the same conditions except for the following changes. For the umbrella sampling simulations, centers of mass (COM) distance restraints with harmonic potentials were applied, while for MD simulations feeding into MM-PBSA computations no restraints were used. For the PMF calculations, 220 ns per umbrella window of restrained MD simulations were conducted resulting in a cumulated simulation time of ~13 μs in total. For the MM-PBSA calculation, 200 ns of unrestrained MD simulations per dimer configuration were performed. If not stated otherwise, the first 40 ns of each umbrella sampling simulation were discarded as prolonged equilibration time of

the TGR5 dimer in the analysis. The same holds for the first 20 ns of the unrestrained MD simulations used for subsequent MM-PBSA computations.

Potential of mean force computations

For the dimerization of TGR5 protomers, the distance *r* between the COM of the C_α atoms of TMs of each protomer was chosen as the reaction coordinate. To reconstruct a potential of mean force from the umbrella sampling[65] simulations, the Weighted Histogram Analysis Method (WHAM)[66,67] was applied. Initially, the protomers were separated with a spacing of 1 Å in between each umbrella window; where a lack of overlap between windows was detected, additional umbrella windows with a 0.5 Å spacing were added (**Figure S1 A and B**). The average spacing between two windows is thus 0.69 Å for the 1/8 and 0.70 Å for the 4/5 interface. A force constant of the harmonic restraining potential of 6 kcal mol^{-1} $Å^{-2}$ was sufficient to restrain the conformations close to the reference point. The final setup is summarized in **Table 1**. The errors at the reference points were calculated with the Monte Carlo bootstrapping method included in the WHAM implementation used here. The convergence of the resulting PMF was checked by calculating PMFs from different portions of the simulations. From 80 ns to the full 220 ns of umbrella sampling, the difference between PMFs decreased with increasing length of the simulations, yielding a maximum difference between PMFs in the step from 210 ns to 220 ns of ~0.4 kcal mol^{-1} for both PMFs (**Figure S1 C and D**).

Table 1. Umbrella sampling windows and associated reaction coordinate for the two dimerization interfaces of TGR5.

Interface	r_{start} [a]	Range (*r*) [a]	Δ*r* [a]	Umbrella windows	Avg. *r*/window [a]
1/8	41.6	34.6 - 57.8	22.8	33	0.69
4/5	34.4	30.9 - 50.5	19.6	28	0.70

[a] In Å.

Estimation of association free energy

From the PMF, the association free energy was estimated similar to ref. [68], following the approach for a two-body membrane system by Johnston *et al.*.[44] In short, the PMF is integrated along the reaction coordinate for dimeric states only. From this, an association constant (K_a; eq. 1) is calculated, which is transformed to the mole fraction scale (K_x; eq. 2) taking into account the number of lipids N_L per surface area A.[69] In our case, the largest simulated system was used to derive the parameters N_L=185 in one leaflet and A = 1.46 × 10^{-4} μm^2. The largest system was used as a reference frame for the number of lipids as this represents the bulk state for the monomeric system. With K_x, the difference in free energy between dimer and monomers (ΔG) is calculated according to eq. 3. In eqs. 1-3, r is the value of the reaction coordinate, $w(r)$ is the PMF at r, r_D is the maximum distance at which the protein is still considered a dimer, r_{min} is the distance at the global minimum of the PMF which was used as a lower boundary for integration, k_B is the Boltzmann constant, and T is the temperature at which the simulations were performed. r_D defines the boundary between monomeric and dimeric states and was derived from the PMF (**Figure 2**) as the midpoint between the global minimum in the free energy profile and the maximum following with increasing r.

$$K_a = \frac{||\Omega||}{(2\pi)^2}\int_{r_{min}}^{r_D} r e^{\frac{-w(r)}{k_B T}} dr \qquad K_x = K_a \frac{N_L}{A} \qquad \Delta G = -RT\, ln(K_x) \qquad \text{eqs. 1-3}$$

Additionally, a factor that considers the restriction of the configurational space of the monomers upon dimer formation is included in terms of the angle sampled between the two chains in the dimeric state (eq. 4) and the accessible rotational space of the monomers, $(2\pi)^2$. A component

perpendicular to the membrane plane does not need to be considered, since the protomers are tightly embedded in the membrane.

$$\left||\Omega|\right| = [\max(\theta_a) - \min(\theta_a)] * [\max(\theta_b) - \min(\theta_b)] \quad \text{eq. 4}$$

In eq. 4, the angle θ_a is defined as the angle formed by the vectors connecting the COM of the TMs of protomer A, the COM of residues 17-42 of TM 1 of protomer A, and the corresponding COM of protomer B. The second angle θ_b was defined in the same manner for protomer B, respectively. The average angle was calculated per umbrella window for dimeric states. The maximum and minimum of theses average angles were used to calculate $||\Omega||$.

MM-PBSA computations

Dimeric configurations at the distances corresponding to the global minima in the PMFs of dimerization were used as starting points for 200 ns of unrestrained MD simulations of both dimers. On snapshots extracted extracted every 40 ps from these simulations and stripped off waters, ions, and lipids, MM-PBSA computations with an implicit membrane model were conducted to obtain a per-residue effective energy contribution to the dimerization of TGR5. The first 20 ns of the MD simulations were not considered.

To accomplish the MM-PBSA computations, we extended the functionality of the program FEW[70] in the AMBER program suite to allow calculations on two proteins with the previously published implicit membrane functionality.[71] A function for correcting the non-polar contribution to the solvation free energy for residues lying inside the membrane plane was introduced and applied. This was necessary because the standard method[72] treats the non-polar term as proportional to the solvent accessible surface area of the residue, which is only valid for residues in a polar

environment such as an aqueous solution. In a hydrophobic environment such as the inside of a phospholipid bilayer, the solvent accessible surface area would have a negligible or even reverse effect on the non-polar contribution.[73] To account for this effect, we neglected the non-polar term for all residues lying inside the hydrophobic area of the implicit membrane model in a frame-wise manner. This added functionality is available as of version 18 of AMBER. Other approaches addressing the question of how to compute the non-polar part of solvation free energy in membrane environments reweight an effective surface tension term by Gaussian-distributed functions proportional to the distance of the atom from the center of the membrane.[73,74] While these methods are expected to model the underlying conditions more realistically, they still require further evaluation and validation in regard to the transferability of the additional parameters to a given system.

For computing the polar part of the solvation free energy, a five-slab membrane model with three dielectric constants ε was used with a total thickness of 38 Å and was placed in accordance with the explicit membrane used in the MD simulations. The dielectric constant of the solute was set to 1, the bulk solvent dielectric to 80. The core membrane slab with a thickness 16 Å was assigned a dielectric constant of 2, and a 6 Å intermediate slab with a dielectric constant of 3 is located on each side of the core slab. The outermost slabs of 5 Å each representing the phospholipid head groups of the bilayer were assigned a dielectric constant of 160.[71,75] Concentrations of 0.15 M of monovalent counterions were used to mimic the conditions in the explicit solvent simulations. FEW uses APBS[76] to calculate the polar term of the solvation free energy and the "draw_membran2" program to create the membrane slabs.[77]

Boundary conditions in APBS were treated by using a focusing approach with three steps, a large grid of 250 Å length, a medium grid of 200 Å length, and a small grid of 150 Å length in all dimensions.

129 grid points in all dimensions were used. Single Debye-Hückel (SDH) boundary conditions were used for the initial focusing step, and a cubic B-spline discretization method was chosen to map charges of the solute to the maps. Dielectric and ion-accessibility coefficients were defined by the molecular surface definitions ("mol" flag) with a 1.4 Å solvent molecule radius and 10 points $Å^{-2}$ sphere density. Because the configurational entropy was not considered in the calculation of binding free energies, as done previously in related computations,[78,79] the sum of all considered contributions is an effective free energy, denoted G_{eff}.

Results

Potentials of mean force of TGR5 dimerization

To compare the two dimerization interfaces of TGR5 (1/8 and 4/5) with respect to dimerization energetics, umbrella sampling simulations and subsequent computations of a PMF of dimerization as a function of the protomer separation distance *r* were conducted. Separating the monomers along their COM axis does not introduce a strain by unnaturally pushing residues into one another, which could happen if, e.g., they were separated perpendicular to this axis. As a free rotation of the protomers is allowed, the protomers can in principle adopt the most favorable orientation along the reaction coordinate. Yet, due to the slow relaxation dynamics of proteins in membranes, e.g., about 20 μs for rhodopsin,[80,81] and sampling times of 220 ns per umbrella window, the sampling of orientational configurations will likely not be converged. Still, the impact of this is expected to be small when comparing free energy profiles of the two TGR5 dimer configurations due to cancellation of errors and because the starting configurations were derived from experimental dimer configurations. To check for the overlap of the frequency distributions of reaction coordinate values, the histograms of umbrella sampling windows were represented by the kernel density. The results show well overlapping histograms (**Figure S1 A and B**), which is a prerequisite for applying WHAM to extract a PMF from these distributions.[67,68] The RMSD to the respective starting structures during each umbrella sampling simulation reached a stable plateau after 40 ns in the individual windows (similar to the RMSD determined in the unbiased simulations; **Figure S2**), and the average RMSD of the backbone atoms indicates overall moderate structural changes in the individual umbrella sampling windows with RMSD ≈ 3.7 Å for the whole protein and ~2.4 Å only considering the transmembrane helices for both dimeric configurations (**Table S1** and **Table S2**). Hence, the first 40 ns of each window were omitted from further analyses. Other studies computing

PMFs of membrane systems also report relaxation times of 30-50 ns, which is in line with our results.[68,82,83] For all simulations, the integrity of the membrane structure and the position of the dimers therein was evaluated in terms of the spatial distribution of the electron density of the membrane components, with systems for both interfaces showing highly similar and evenly distributed electron densities (**Figure S3**). Repeating the computations of the PMFs for parts of the simulation time demonstrated that, for both systems, the PMFs are converged after ~200 ns of simulation time per window (**Figure S1**). The error in the PMFs estimated from a bootstrap sampling is overall small with a maximum of 0.16 kcal mol^{-1} in the region $r > 50$ Å for the 1/8 interface (**Figure 2**). For reasons of comparison, the PMF values at $r = 50$ Å and 58 Å, the monomeric states (states C and F in **Figure 2**) for the 4/5 and 1/8 configurations, respectively, were set to zero.

The PMF of dimerization via the 1/8 interface has a global minimum of -8.1 kcal mol^{-1} at $r = 35.8$ Å (state D in **Figure 2**). For the 4/5 interface, the PMF has a global minimum of -6.4 kcal mol^{-1} at $r = 33.8$ Å (state A in **Figure 2**). The initial model with the 4/5 interface with $r = 34.5$ Å generated by superimposition of the TGR5 protomers onto the dimer structure of 3ODU[29] was already close to the global minimum of the PMF, while the starting model with the 1/8 interface generated with the dimer structure of 4DJH[28] was located at $r = 40.5$ Å. The distance disparity in the 1/8 interface model could be caused by the structural difference between the homology model of the TGR5 protomer and the κ-opioid receptor (C_α atom RMSD of equivalent atoms = 5.0 Å), or the membrane environment of TGR5, which was not present in the crystallization of the template.[28]

The configurational free energy for the 1/8 interface increases with increasing r until it reaches a local maximum of ~0 kcal mol^{-1} at $r \approx 47$ Å (state F in **Figure 2**). This smooth increase in the energy is likely caused by helices 8 sliding along each other upon separation and by TM1 becoming

more perpendicular with respect to the membrane plane, which helps maintain interface interactions over a larger *r* range and prevents the formation of lipid-filled pockets between the protomers (**Figure 2**). In contrast, the configurational free energy for the 4/5 interface rises much more steeply and reaches a global maximum of ~3.3 kcal mol^{-1} at $r \approx 49$ Å (state B in **Figure 2**). Apparently, the formation of protein-lipid interactions between both protomers and lipids that slipped in between are more disfavorable for the dimer with 4/5 interface (state B in **Figure 2**) than the gentle release of protein-protein interactions for the dimer with 1/8 interface (state E in **Figure 2**); in the latter case, the density of lipids in between both protomers is much smaller because of the interactions between helices 8, which act similar to two approaching wedges separating the lipids between the protomers. In the shallow basins between B and C (E and F), the protomers form an increasing number of contacts with decreasing *r* up until a high (low) number of lipids have to be displaced in order to establish an interface contact resulting in a high (low) energy barrier for the 4/5 (1/8) interface. Finally, at $r = 50$ Å and 58 Å, the configurational free energies reach 0 kcal mol^{-1}, related to a complete separation of the two dimers (states C and F, respectively, in **Figure 2**).

As the $Y111A^{3.51}$ variant shows no multimerization of TGR5,[24] the role of $Y111^{3.51}$ in the 4/5 interface is highly interesting. In this interface, $Y111^{3.51}$ almost exclusively interacts with its symmetric counterpart at close *r* (32 Å to 36 Å) (**Figure 3 A, B and C**), while at a larger separation of the two protomers ($r > 38$ Å), it forms hydrogen bonds to the head group moiety of bridging DOPC lipids. At the intermediate distance of $r = 36$ Å to 38 Å still related to a dimeric configuration, both $Y111^{3.51}$ are bridged by exactly one DOPC molecule in a large fraction of the snapshots (**Figure 3 B and D**). Thus, $Y111^{3.51}$ indirectly mediates interactions between the

protomers even if no direct contact is present. This could explain, why the Y111A$^{3.51}$ variant abolishes TGR5 oligomerization by preventing the formation of the 4/5 interface.

To conclude, the PMFs of TGR5 dimerization show that either interface formation is favorable and that the 1/8 interface identified in live cell FRET experiments[24] shows a smoother dimerization free energy profile than the 4/5 interface. This is caused by an energetically unfavorable lipid-filled pocket formation during the association of the 4/5 interface. Furthermore, Y111$^{3.51}$ plays a vital role in the formation of the 4/5 interface by either forming hydrogen bonds with its counterpart in the other protomer or with head group moieties of DOPC lipids over an extended distance range.

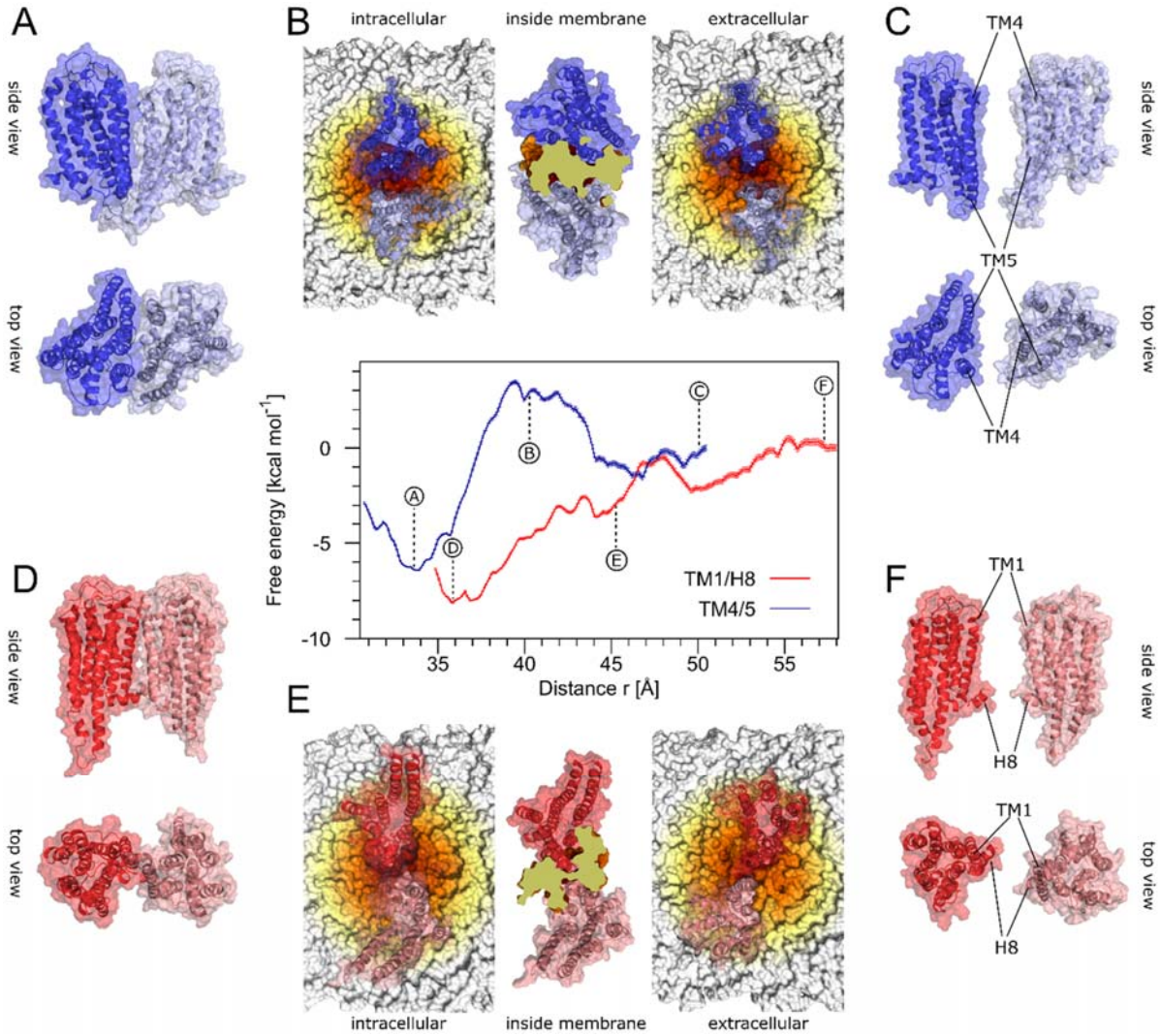

Figure 2. The two dimeric configurations of TGR5 and the PMFs of dimerization. Center: PMFs of TGR5 dimerization (red: 1/8 interface; blue: 4/5 interface) calculated from umbrella sampling simulations; error bars were determined according to the bootstrap error estimation in the WHAM implementation used here. The curves were aligned to a value of 0 kcal mol^{-1} at the largest value of the reaction coordinate, considering the dimers dissociated at these points. Letters in circles correspond to structures shown in panels A-F. Dimeric configurations of TGR5 with 4/5 interface at the global minimum (**A**) and the dissociated state (**C**) are shown in a side view or top view (looking from the extracellular side) perspective. **D** and **F** show the respective structures for TGR5 with 1/8 interface. In the case of the 4/5 interface, the barrier in the PMF coincides with the formation of a layer of lipids between the protomers, which bind into cavities in the dimerization interface (**B**). The 1/8 interface on the other hand is wedge-shaped owing to H8 and TM1, which occludes lipids from the dimerization interface (**E**). Lipids are colored from red to yellow and white according to their distance to the COM of the two TGR5 protomers.

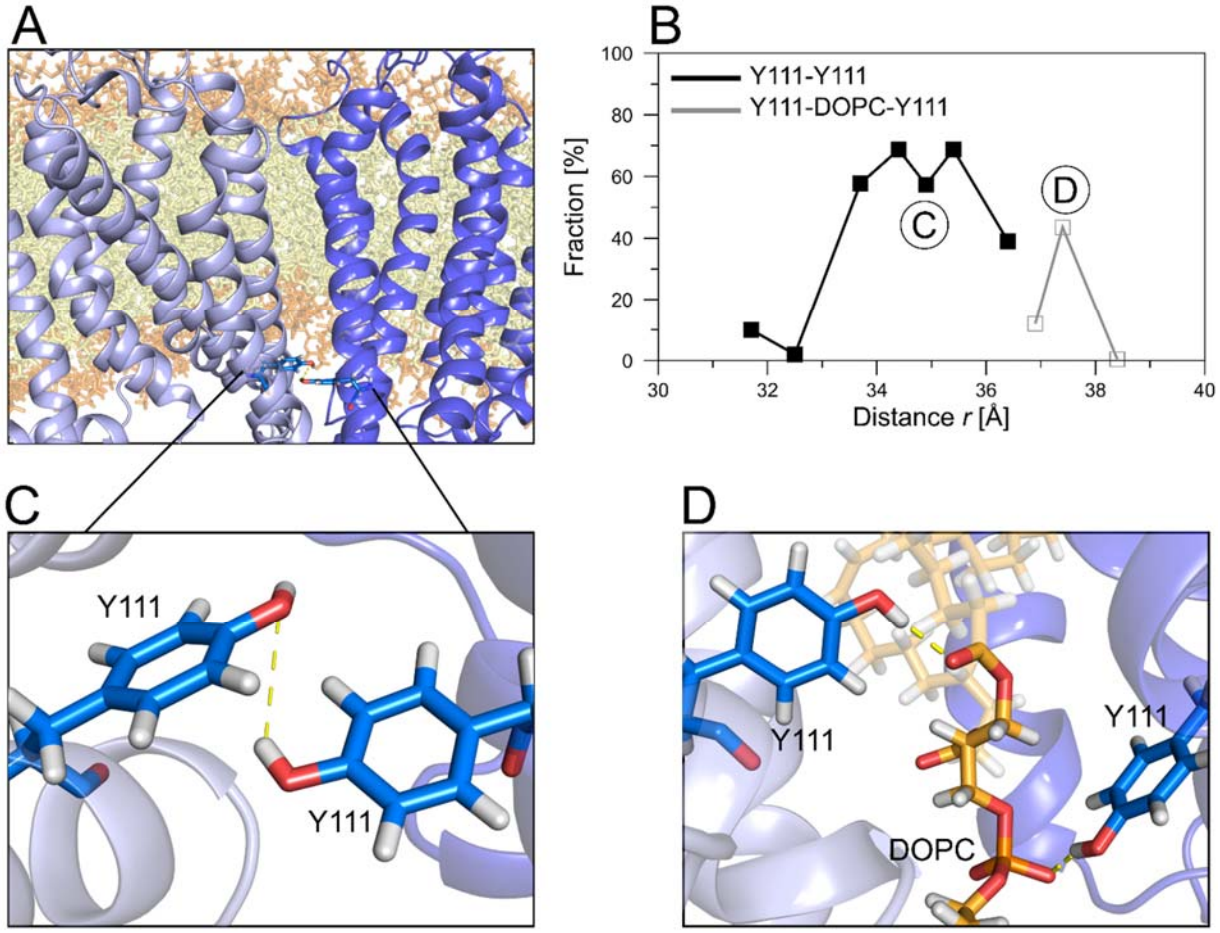

Figure 3: Interactions of Y111$^{3.51}$ in the 4/5 interface. A, **C:** At close distance r, both Y111$^{3.51}$ residues form a hydrogen bond across the dimer interface. **B:** The fraction of the corresponding simulations from umbrella sampling are shown in which a Y111-Y111 hydrogen bond (black line, related to panel C) or a hydrogen bond to the one bridging DOPC molecule (**D**) is present (grey line).

Constants and free energies of association

From the PMFs, constants and free energies of association were calculated according to eqs. 1-4, applying the integration boundaries r_{min} and r_D (**Table 2**). In doing so, the restriction of the configurational space in the dimeric state compared to two freely rotating protomers in the membrane was considered (**Table 2**):[84] For freely rotating protomers in the membrane plane, the accessible rotational space is $||\Omega|| = (2\pi)^2$, while $||\Omega|| = 0.17$ and 0.1 for the 1/8 and 4/5 interface, respectively, in the dimeric configurations. The resulting K_x and ΔG (**Table 2**) relate to a state of

one TGR5 dimer in a membrane of 369 lipids, according to our simulation setup. A direct comparison to dissociation constants determined by live cell FRET experiments is not possible due to the arbitrary definition of the association constant K_{D1} there, which relates to the initial dimerization of the receptor via the primary 1/8 interface;[24] an explicit determination of K_{D1} was not possible in these experiments. With respect to K_{D1}, K_{D2}, which relates to the dimerization of TGR5 dimers via a secondary interface, is seven-fold larger,[24] demonstrating a weaker association via the secondary interface than the primary one. Our results qualitatively agree with this finding in that K_x of the 1/8 interface is larger than that of the 4/5 interface (**Table 2**). Furthermore, on a quantitative level, the ratio of K_x's determined here is ~40, which is within a factor of ~6 to the ratio of the experimentally determined K_D's[24] and, hence, within chemical accuracy at $T \approx 300$ K (**Table 2**). This comparison lends remarkable support to the quality of the setup, parameterization, and execution of our simulations.

To conclude, the calculated association constants for the respective interfaces show that the formation of the 1/8 interface is more favorable than that of the 4/5 interface, concordant with results of live cell FRET experiments.[24] Additionally, the ratio of the calculated association constants is within chemical accuracy to the experimentally determined ratio.[24]

Table 2. Thermodynamic quantities for each TGR5 dimer system.[a]

Interface	**1/8**	**4/5**
$\|\|\boldsymbol{\Omega}\|\|$ **[rad]**	0.17	0.10
$\boldsymbol{r_{min}}$ **[Å]**	35.8	33.8
$\boldsymbol{r_D}$ **[Å]**	40.6	36.8
$\boldsymbol{K_a}$ **[µm²]**	2.1×10^{-3}	5.3×10^{-5}
$\boldsymbol{K_x}$	5.3×10^{3}	1.3×10^{2}
$\boldsymbol{\Delta G}$ **[kcal mol^{-1}]**	-4.7	-2.5

[a] K_a, K_x, ΔG, and $||\Omega||$ were computed according to eqs. 1-4.

Per-residue decomposition of effective binding energies

To complement the previous investigations of TGR5 dimerization, the MM-PBSA approach considering an implicit solvent and implicit membrane environment in connection with a structural decomposition of the effective binding energy on a per-residue level[85,86] was used to reveal putative regions of strong interactions ("hot spots") in the dimer interfaces. These hot spot residues can be exploited in a knowledge-driven approach by identifying small molecules that mimic those residues and, thus, act as dimerization inhibitors.[86] For this, MD simulations of 200 ns length were conducted (of which the last 180 ns were used for MM-PBSA analysis) at a separation distance corresponding to the global minimum of the respective PMFs. Within the timescale of our simulations, the dimers do not dissociate and only show small local conformational changes, which is reflected by RMSD values with respect to the starting structure in the 3-4.5 Å range for the protomers in both dimer configurations (**Figure S2**). Over the simulation time, the total effective energy of binding calculated by the MM-PBSA single trajectory approach (ΔG_{eff}) remains largely stable with a slow drift towards lower energies as indicated by the slope of the linear regression function of -0.0584 kcal mol^{-1} ns^{-1} for the 1/8 and -0.0858 kcal mol^{-1} ns^{-1} for the 4/5 interface (**Figure S4**). Still, ΔG_{eff} fluctuates between -45 and -90 kcal mol^{-1} for the 1/8 interface and -65 to -160 kcal mol^{-1} for the 4/5 interface (**Figure S4**). Both the magnitudes of these values and the fluctuations are well within the ranges reported in similar studies.[86-88] From ΔG_{eff} values alone, the 4/5 interface appears to be more favorable than the 1/8 interface. Note, however, that we did not consider configurational entropy contributions in the MM-PBSA computations, in order to avoid introducing additional uncertainty in the computations.[87,89,90] Such contributions can have a pronounced effect, as, e.g., indicated by the $||\Omega||$ values computed above (**Table 2**), where the restriction of the rotational space of the monomers disfavors formation of the 4/5 interface more than that of the 1/8 interface.

According to previous studies[79,86] only residues *i* with $\Delta G_{\text{eff},i} < -2$ kcal mol^{-1} were considered hot spots. As expected, the hot spot residues identified for both interfaces are highly symmetrically distributed in both protomers (**Figure 4**). Notably, residues located at the intracellular ends of helices and the respective adjacent loops were found to have the lowest $\Delta G_{\text{eff},i}$. Here, it is energetically favorable for the solvent-exposed hydrophobic residues to form interactions with one another, which is reflected by, on average, 2.7 kcal mol^{-1} more favorable non-polar solvation energies of such residues compared to hydrophobic residues in the membrane. Projections of $\Delta G_{\text{eff},i}$ onto TGR5 protomers are shown in **Figure 4**.

In the 4/5 interface, the residues with the highest contributions to the effective binding energy are mainly hydrophobic with the exception of H193$^{5.67}$ at the intracellular and Y167$^{5.41}$ at the extracellular end of TM 5 located in the polar head group regions (**Figure 4 A, B**). Y171$^{5.45}$ is the only polar residue that is located in the center of the dimerization interface. In TM4 and the intracellular loop 2 between TM3 and TM4, several residues contribute highly favorably to binding, including several proline residues (P117^{IL2}, P120$^{4.38}$, P121$^{4.39}$) as well as M112$^{3.52}$, L115$^{3.55}$, and L126$^{4.44}$. Y111$^{3.51}$ yields $\Delta G_{\text{eff},i}$ = -1.76 kcal mol $^{-1}$. Although lower than the -2 kcal mol^{-1} cut-off chosen to define hot spots, mutation of this residue to alanine is expected to reduce TGR5 dimer formation via the 4/5 interface by ~20 times at T = 300 K, corroborating the above structural findings of its importance for interface formation.

In the parts of the 1/8 interface located in the hydrophobic region of the membrane, hot spots are mainly small and / or hydrophobic residues, such as G16$^{1.34}$, L18$^{1.36}$, L20$^{1.38}$, L282$^{7.55}$ and W291$^{8.54}$ (**Figure 4 C, D**). In the polar interface regions near the phosphate head groups, charged amino acids K15$^{1.33}$ at the N-terminal end of helix 1 and R292$^{8.55}$ at the C-terminal end of helix 8 are hot spots. The cluster of hot spot residues on TM1 (G16$^{1.34}$, L18$^{1.36}$, L20$^{1.38}$) could allow the design of

an inhibitory peptide or peptide mimetic,[91-94] which mimics the hot spot residues to disrupt the interface formation.

To conclude, we identified hot spot residues in the 1/8 and 4/5 interfaces, of which three form a cluster in TM1.

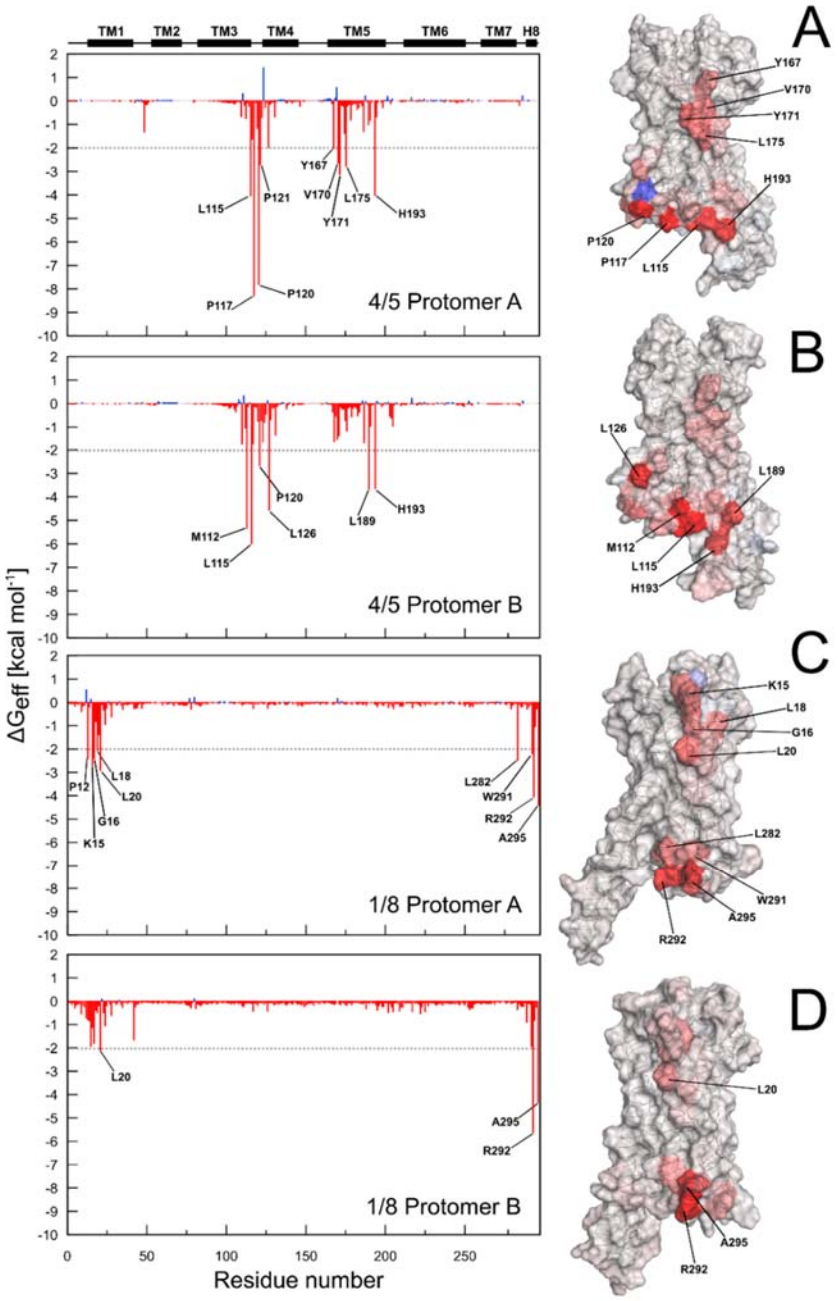

Figure 4. Per-residue decomposition of effective MM-PBSA binding energies for both TGR5 dimer interfaces. The distribution of hot spot residues for the first (**A**) and second (**B**) protomer of the 4/5 interface is shown as a graph and projected onto the structure, also for the first (**C**) and second (**D**) protomer of the 1/8 interface. Residues with $\Delta G_{\mathrm{eff},i} < -2$ kcal mol^{-1} (indicated by a dotted gray line) are considered hot spots. The standard error of the mean is < 0.1 kcal mol^{-1} for each residue; secondary structure of the TGR5 model is displayed at the top of the bar plots with black boxes showing α-helices. For the projections of $\Delta G_{\mathrm{eff},i}$, a representative structure of a TGR5 protomer from the MD simulations used for these calculations is used, and residues are colored from red (-9 kcal mol^{-1}) to white (0 kcal mol^{-1}) to blue (4 kcal mol^{-1}).

Discussion

In this study, we have shown by PMF computations based on MD simulations at the atomistic level and subsequent computations of constants and free energies of association that the formation of both the 1/8 and 4/5 interface is energetically favorable for TGR5, and that formation of the 1/8 interface is favored over that of the 4/5 interface. Both results are in line with our previous experimental findings,[24] where FRET experiments in live cells showed that the 1/8 interface of TGR5 is the primary dimerization interface. Furthermore, FRET distances derived from models of dimers of dimers indicated the presence of either the 4/5 or 5/6 interface as a secondary interface. Here, by modeling of respective dimer configurations of TGR5 in the active state, together with experimental findings that the activation of TGR5 does not influence its oligomerization,[24] we ruled out the presence of the 5/6 interface. Hence, our results suggest that the 4/5 interface is the secondary interface for TGR5 oligomer formation.

Structural analyses of TGR5 dimer configurations related to characteristic points in the PMFs revealed the formation of a lipid-filled pocket when TGR5 molecules approach to form the 4/5 configuration. Associated with this is an energy barrier of ~3.3 kcal mol^{-1}, indicating that this lipid-separated/lipid-bridged TGR5 dimer state is disfavorable. In comparison, in the 1/8 interface, the two wedge-shaped interfaces can separate the lipid layer between the protomers more easily, which results in a smaller energy barrier and smoother free energy profile. As a consequence, more lipid-separated/lipid-bridged TGR5 dimer configurations are accessible in the latter case, which directly relates to the larger K_x (or lower ΔG) via the integration in eq. 1. As such, our computations indicate that differences in lipid-protein interactions contribute to the experimentally observed and computed differences in constants and free energies of association. This is in line with other studies, which showed an impact of the local lipid composition on the association of GPRCs.[95-98] We computed ΔG values (**Table 3**) that are comparable in magnitude to previous studies of GPCR

dimerization with similar setups [33,44] and experimental studies on protein-protein interactions in lipid bilayers. [99,100] A direct comparison to dissociation constants determined by live cell FRET experiments is not possible because the association constant K_{D1} there, which relates to the initial dimerization of the receptor via the primary 1/8 interface, was fixed at an arbitrary value.[24] Factors that might influence the magnitude of our computed ΔG are not precise enough starting configurations of dimeric TGR5, angular distributions of the bound state used for calculating the correction term $||\Omega||$ (eq. 4) that are too narrow due to insufficient sampling, and imbalanced protein-lipid, protein-protein, and lipid-lipid interactions.

Application of the MM-PBSA method to study protein-protein interactions and identify hot spot residues[79,101] using an implicit solvent is well established.[102] By using MM-PBSA computations with an additional implicit membrane representation,[70,71] we identified several hot spot residues that are specific for both interfaces of TGR5. Most of the hot spot residues are clustered at the polar interface regions near the phosphate head groups. This allows for the design of small-molecule inhibitors of dimerization, exploiting strategies developed by us[78,85,103] and others[104-106] to translate knowledge about the location and orientation of hot spots into a molecular design. Similarly, self-inserting peptides mimicking TMs have been successfully employed to inhibit the dimerization of GPCRs.[91-93,107,108] Furthermore, knowledge of hot spot residues that are specific for the interfaces could be utilized to disrupt the dimerization upon mutation to alanine to probe the physiological effect of TGR5 interactions via specific interfaces, as done before for other GPCRs.[108]

Finally, we determined that Y111$^{3.51}$ plays an important role in the formation of the 4/5 interface. Y111$^{3.51}$, which is part of the conserved (D/E)RY motif,[27] is involved markedly in the dimer formation. As of now, no explanation for the function of this residue was provided, which in all GPCR X-ray crystal structures points towards the membrane environment.[27-29] Our findings that

Y111$^{3.51}$ mediates direct interactions between the TGR5 protomers and forms lipid-mediated interactions over an extended range of the dimerization pathway are in line with experimental findings that the Y111A$^{3.51}$ variant of TGR5 does not form multimers anymore.[24] The role of Y111 in TGR5 association is furthermore underscored by our MM-PBSA results.

In summary, we described the first extensive energetic evaluation of GPCR dimerization on the atomistic level and provided the structural foundation for developing small-molecule inhibitors of or performing mutational analyses on TGR5 dimerization. The types of computations should be transferable to other transmembrane proteins that form dimers or higher oligomers as long as good structural models of the dimeric or oligomeric states are available. Such computations may help to overcome current restrictions due to an imperfect energetic representation of protein association at the coarse-grained level.[41,42]

Acknowledgments

This study was funded by the “Forschungskommission” (FOKO) of the Medical Faculty of the Heinrich Heine University Düsseldorf. Part of the work of VK was funded by the Deutsche Forschungsgemeinschaft (DFG, German Research Foundation) – Projektnummer 190586431 – SFB 974 “Communication and Systems Relevance in Liver Injury and Regeneration“ (Düsseldorf, Germany) (project B01). HG is grateful for computational support and infrastructure provided by the “Zentrum für Informations- und Medientechnologie” (ZIM) at the Heinrich Heine University Düsseldorf and the computing time provided by the John von Neumann Institute for Computing (NIC) on the supercomputer JURECA at Jülich Supercomputing Centre (JSC) (user IDs: HKF7, HDD15; project IDs: 10766, 11761).

References

1. Maruyama, T.; Tanaka, K.; Suzuki, J.; Miyoshi, H.; Harada, N.; Nakamura, T.; Miyamoto, Y.; Kanatani, A.; Tamai, Y. J Endocrinol 2006, 191(1), 197-205.
2. Maruyama, T.; Miyamoto, Y.; Nakamura, T.; Tamai, Y.; Okada, H.; Sugiyama, E.; Nakamura, T.; Itadani, H.; Tanaka, K. Biochem Biophys Res Commun 2002, 298(5), 714-719.
3. Kawamata, Y.; Fujii, R.; Hosoya, M.; Harada, M.; Yoshida, H.; Miwa, M.; Fukusumi, S.; Habata, Y.; Itoh, T.; Shintani, Y. J Biol Chem 2003, 278(11), 9435-9440.
4. Keitel, V.; Görg, B.; Bidmon, H. J.; Zemtsova, I.; Spomer, L.; Zilles, K.; Häussinger, D. Glia 2010, 58(15), 1794-1805.
5. Gertzen, C. G. W.; Spomer, L.; Smits, S. H.; Haussinger, D.; Keitel, V.; Gohlke, H. Eur J Med Chem 2015, 104, 57-72.
6. Sato, H.; Macchiarulo, A.; Thomas, C.; Gioiello, A.; Une, M.; Hofmann, A. F.; Saladin, R.; Schoonjans, K.; Pellicciari, R.; Auwerx, J. J Med Chem 2008, 51(6), 1831-1841.
7. Keitel, V.; Donner, M.; Winandy, S.; Kubitz, R.; Häussinger, D. Biochem Biophys Res Commun 2008, 372(1), 78-84.
8. Keitel, V.; Reinehr, R.; Reich, M.; Sommerfeld, A.; Cupisti, K.; Knoefel, W. T.; Häussinger, D. Z Gastroenterol 2012, 50(01), P5_24.
9. Cao, W.; Tian, W.; Hong, J.; Li, D.; Tavares, R.; Noble, L.; Moss, S. F.; Resnick, M. B. Am J Physiol Gastrointest Liver Physiol 2013, 304(4), G322-327.
10. Hong, J.; Behar, J.; Wands, J.; Resnick, M.; Wang, L. J.; DeLellis, R. A.; Lambeth, D.; Souza, R. F.; Spechler, S. J.; Cao, W. Gut 2010, 59(2), 170-180.
11. Keitel, V.; Reinehr, R.; Gatsios, P.; Rupprecht, C.; Görg, B.; Selbach, O.; Häussinger, D.; Kubitz, R. Hepatology 2007, 45(3), 695-704.
12. Keitel, V.; Cupisti, K.; Ullmer, C.; Knoefel, W. T.; Kubitz, R.; Häussinger, D. Hepatology 2009, 50(3), 861-870.
13. Hov, J. R.; Keitel, V.; Laerdahl, J. K.; Spomer, L.; Ellinghaus, E.; ElSharawy, A.; Melum, E.; Boberg, K. M.; Manke, T.; Balschun, T.; Schramm, C.; Bergquist, A.; Weismueller, T.; Gotthardt, D.; Rust, C.; Henckaerts, L.; Onnie, C. M.; Weersma, R. K.; Sterneck, M.; Teufel, A.; Runz, H.; Stiehl, A.; Ponsioen, C. Y.; Wijmenga, C.; Vatn, M. H.; Stokkers, P. C. F.; Vermeire, S.; Mathew, C. G.; Lie, B. A.; Beuers, U.; Manns, M. P.; Schreiber, S.; Schrumpf, E.; Haeussinger, D.; Franke, A.; Karlsen, T. H.; Grp, I. S. PLOS ONE 2010, 5(8).
14. Yasuda, H.; Hirata, S.; Inoue, K.; Mashima, H.; Ohnishi, H.; Yoshiba, M. Biochem Biophys Res Commun 2007, 354(1), 154-159.
15. McDonald, J. J Gastroenterol Hepatol 1999, 14(6), 515-518.
16. Hiller, C.; Kühhorn, J.; Gmeiner, P. J Med Chem 2013, 56(17), 6542-6559.
17. Tabor, A.; Weisenburger, S.; Banerjee, A.; Purkayastha, N.; Kaindl, J. M.; Hübner, H.; Wei, L.; Grömer, T. W.; Kornhuber, J.; Tschammer, N.; Birdsall, N. J. M.; Mashanov, G. I.; Sandoghdar, V.; Gmeiner, P. Sci Rep 2016, 6, 33233.
18. Hu, J.; Thor, D.; Zhou, Y.; Liu, T.; Wang, Y.; McMillin, S. M.; Mistry, R.; Challiss, R. A. J.; Costanzi, S.; Wess, J. FASEB J 2012, 26(2), 604-616.
19. Taddese, B.; Simpson, L. M.; Wall, I. D.; Blaney, F. E.; Kidley, N. J.; Clark, H. S. X.; Smith, R. E.; Upton, G. J. G.; Gouldson, P. R.; Psaroudakis, G.; Bywater, R. P.; Reynolds, C. A. Biochem Soc Trans 2012, 40, 394-399.
20. Lavoie, C.; Mercier, J.; Salahpour, A.; Umapathy, D.; Breit, A.; Villeneuve, L.; Zhu, W.; Xiao, R.; Lakatta, E.; Bouvier, M. J Biol Chem 2002, 277(38), 35402 - 35410.
21. Hasbi, A.; Perreault, M. L.; Shen, M. Y. F.; Zhang, L.; To, R.; Fan, T.; Nguyen, T.; Ji, X.; O'Dowd, B. F.; George, S. R. FASEB J 2014, 28, 4806-4820.

22. Milligan, G. Mol Pharmacol 2004, 66(1), 1-7.
23. Teichmann, A.; Gibert, A.; Lampe, A.; Grzesik, P.; Rutz, C.; Furkert, J.; Schmoranzer, J.; Krause, G.; Wiesner, B.; Schülein, R. J Biol Chem 2014, 289(35), 24250-24262.
24. Greife, A.; Felekyan, S.; Ma, Q.; Gertzen, C. G. W.; Spomer, L.; Dimura, M.; Peulen, T. O.; Wöhler, C.; Häussinger, D.; Gohlke, H.; Keitel, V.; Seidel, C. A. M. Sci Rep 2016, 6, 36792.
25. Ballesteros, J. A.; Weinstein, H. In Methods in neurosciences; Elsevier, 1995, p 366-428.
26. Isberg, V.; Mordalski, S.; Munk, C.; Rataj, K.; Harpsøe, K.; Hauser, A. S.; Vroling, B.; Bojarski, A. J.; Vriend, G.; Gloriam, D. E. Nucleic Acids Res 2015, 44(D1), D356-D364.
27. Katritch, V.; Cherezov, V.; Stevens, R. C. Annu Rev Pharmacol Toxicol 2013, 53, 531-556.
28. Wu, H.; Wacker, D.; Mileni, M.; Katritch, V.; Han, G. W.; Vardy, E.; Liu, W.; Thompson, A. A.; Huang, X.-P.; Carroll, F. I. Nature 2012, 485(7398), 327.
29. Wu, B.; Chien, E. Y.; Mol, C. D.; Fenalti, G.; Liu, W.; Katritch, V.; Abagyan, R.; Brooun, A.; Wells, P.; Bi, F. C. Science 2010, 330(6007), 1066-1071.
30. Manglik, A.; Kruse, A. C.; Kobilka, T. S.; Thian, F. S.; Mathiesen, J. M.; Sunahara, R. K.; Pardo, L.; Weis, W. I.; Kobilka, B. K.; Granier, S. Nature 2012, 485(7398), 321.
31. Pluhackova, K.; Gahbauer, S.; Kranz, F.; Wassenaar, T. A.; Böckmann, R. A. PLOS Comput Biol 2016, 12(11), e1005169.
32. Prasanna, X.; Sengupta, D.; Chattopadhyay, A. Sci Rep 2016, 6, 31858.
33. Provasi, D.; Boz, M. B.; Johnston, J. M.; Filizola, M. PLOS Comput Biol 2015, 11(3), e1004148.
34. Di Marino, D.; Motta, S.; Limongelli, V. Biophys J 2019, 116(3), 344a.
35. Carpenter, T. S.; López, C. A.; Neale, C.; Montour, C.; Ingólfsson, H. I.; Di Natale, F.; Lightstone, F. C.; Gnanakaran, S. J Chem Theory Comput 2018, 14(11), 6050-6062.
36. Uusitalo, J. J.; Ingólfsson, H. I.; Marrink, S. J.; Faustino, I. Biophys J 2018, 114(3), 437a.
37. Wu, H.; Wolynes, P. G.; Papoian, G. A. J Phys Chem B 2018, 122(49), 11115-11125.
38. Uhlig, F.; Zeman, J.; Smiatek, J.; Holm, C. J Chem Theory Comput 2018, 14(3), 1471-1486.
39. Sejdiu, B. I.; Tieleman, D. P. Biophys J 2018, 114(3), 617a.
40. Pak, A. J.; Dannenhoffer-Lafage, T.; Madsen, J. J.; Voth, G. A. J Chem Theory Comput 2019.
41. Baaden, M.; Marrink, S. J. Curr Opin Struct Biol 2013, 23(6), 878-886.
42. Javanainen, M.; Martinez-Seara, H.; Vattulainen, I. PLOS ONE 2017, 12(11), e0187936.
43. Woo, H.-J.; Roux, B. Proc Natl Acad Sci U S A 2005, 102(19), 6825-6830.
44. Johnston, J. M.; Wang, H.; Provasi, D.; Filizola, M. PLOS Comput Biol 2012, 8(8), e1002649.
45. Sun, H.; Li, Y.; Tian, S.; Wang, J.; Hou, T. PLOS Comput Biol 2014, 10(7), e1003729.
46. Sun, H.; Chen, P.; Li, D.; Li, Y.; Hou, T. J Chem Theory Comput 2016, 12(2), 851-860.
47. Rasmussen, S. G.; DeVree, B. T.; Zou, Y.; Kruse, A. C.; Chung, K. Y.; Kobilka, T. S.; Thian, F. S.; Chae, P. S.; Pardon, E.; Calinski, D. Nature 2011, 477(7366), 549.
48. Tautermann, C. S.; Pautsch, A. ACS Med Chem Lett 2011, 2(6), 414-418.
49. Dror, R. O.; Arlow, D. H.; Maragakis, P.; Mildorf, T. J.; Pan, A. C.; Xu, H.; Borhani, D. W.; Shaw, D. E. Proc Natl Acad Sci U S A 2011, 108(46), 18684-18689.
50. Eswar, N.; Eramian, D.; Webb, B.; Shen, M.-Y.; Sali, A. In Structural proteomics; Springer, 2008, p 145-159.
51. Cvejic, S.; Devi, L. A. J Biol Chem 1997, 272(43), 26959-26964.

52. Lomize, M. A.; Lomize, A. L.; Pogozheva, I. D.; Mosberg, H. I. Bioinformatics 2006, 22(5), 623-625.
53. Jo, S.; Kim, T.; Iyer, V. G.; Im, W. J Comput Chem 2008, 29(11), 1859-1865.
54. Domanski, J.; Stansfeld, P. J.; Sansom, M. S.; Beckstein, O. J Membr Biol 2010, 236(3), 255-258.
55. Jo, S.; Kim, T.; Im, W. PLOS ONE 2007, 2(9), e880.
56. Jorgensen, W. L.; Chandrasekhar, J.; Madura, J. D.; Impey, R. W.; Klein, M. L. J Chem Phys 1983, 79(2), 926-935.
57. D.A. Case, V. B., J.T. Berryman, R.M. Betz, Q. Cai, D.S. Cerutti, T.E. Cheatham, III, T.A. Darden, R.E.; Duke, H. G., A.W. Goetz, S. Gusarov, N. Homeyer, P. Janowski, J. Kaus, I. Kolossváry, A. Kovalenko,; T.S. Lee, S. L., T. Luchko, R. Luo, B. Madej, K.M. Merz, F. Paesani, D.R. Roe, A. Roitberg, C. Sagui,; R. Salomon-Ferrer, G. S., C.L. Simmerling, W. Smith, J. Swails, R.C. Walker, J. Wang, R.M. Wolf, X.; Kollman, W. a. P. A.: University of California, San Francisco, 2014.
58. Maier, J. A.; Martinez, C.; Kasavajhala, K.; Wickstrom, L.; Hauser, K. E.; Simmerling, C. J Chem Theory Comput 2015, 11(8), 3696-3713.
59. Dickson, C. J.; Madej, B. D.; Skjevik, A. A.; Betz, R. M.; Teigen, K.; Gould, I. R.; Walker, R. C. J Chem Theory Comput 2014, 10(2), 865-879.
60. Joung, I. S.; Cheatham III, T. E. J Phys Chem B 2008, 112(30), 9020-9041.
61. Joung, I. S.; Cheatham III, T. E. J Phys Chem B 2009, 113(40), 13279-13290.
62. Cheatham, T. E., III; Miller, J. L.; Fox, T.; Darden, T. A.; Kollman, P. A. J Am Chem Soc 1995, 117(14), 4193-4194.
63. Ryckaert, J.-P.; Ciccotti, G.; Berendsen, H. J. C. J Comput Phys 1977, 23(3), 327-341.
64. Salomon-Ferrer, R.; Götz, A. W.; Poole, D.; Le Grand, S.; Walker, R. C. J Chem Theory Comput 2013, 9(9), 3878-3888.
65. Torrie, G. M.; Valleau, J. P. J Chem Phys 1977, 66(4), 1402-1408.
66. Kumar, S.; Rosenberg, J. M.; Bouzida, D.; Swendsen, R. H.; Kollman, P. A. J Comput Chem 1995, 16(11), 1339-1350.
67. Kumar, S.; Rosenberg, J. M.; Bouzida, D.; Swendsen, R. H.; Kollman, P. A. J Comput Chem 1992, 13(8), 1011-1021.
68. Pagani, G.; Gohlke, H. Sci Rep 2018, 8(1), 5733.
69. Fleming, K. G. J Mol Biol 2002, 323(3), 563-571.
70. Homeyer, N.; Gohlke, H. J Comput Chem 2013, 34(11), 965-973.
71. Homeyer, N.; Gohlke, H. Biochim Biophys Acta 2015, 1850(5), 972-982.
72. Sitkoff, D.; Sharp, K. A.; Honig, B. J Phys Chem 1994, 98(7), 1978-1988.
73. Ulmschneider, M. B.; Ulmschneider, J. P.; Sansom, M. S.; Di Nola, A. Biophys J 2007, 92(7), 2338-2349.
74. Ulmschneider, J. P.; Ulmschneider, M. B. J Chem Theory Comput 2007, 3(6), 2335-2346.
75. Stern, H. A.; Feller, S. E. J Chem Phys 2003, 118(7), 3401-3412.
76. Baker, N. A.; Sept, D.; Joseph, S.; Holst, M. J.; McCammon, J. A. Proc Natl Acad Sci U S A 2001, 98(18), 10037-10041.
77. Grabe, M.: Pittsburgh, PA, USA, 2008.
78. Metz, A.; Schanda, J.; Grez, M.; Wichmann, C.; Gohlke, H. J Chem Inf Model 2013, 53(9), 2197-2202.
79. Ciglia, E.; Vergin, J.; Reimann, S.; Smits, S. H.; Schmitt, L.; Groth, G.; Gohlke, H. PLOS ONE 2014, 9(4), e96031.

80. Naqvi, K. R.; Gonzalez-Rodriguez, J.; Cherry, R.; Chapman, D. Nature New Biol 1973, 245(147), 249.
81. Cherry, R. J. Biochim Biophys Acta Rev Biomembr 1979, 559(4), 289-327.
82. Mukherjee, S.; Kar, R. K.; Nanga, R. P. R.; Mroue, K. H.; Ramamoorthy, A.; Bhunia, A. Phys Chem Chem Phys 2017, 19(29), 19289-19299.
83. Selyutina, O. Y.; Apanasenko, I.; Kim, A.; Shelepova, E.; Khalikov, S.; Polyakov, N. Colloids Surf B Biointerfaces 2016, 147, 459-466.
84. Johnston, J. M.; Wang, H.; Provasi, D.; Filizola, M. PLOS Comput Biol 2012, 8.
85. Gohlke, H.; Kiel, C.; Case, D. A. J Mol Biol 2003, 330(4), 891-913.
86. Metz, A.; Pfleger, C.; Kopitz, H.; Pfeiffer-Marek, S.; Baringhaus, K. H.; Gohlke, H. J Chem Inf Model 2012, 52(1), 120-133.
87. Gohlke, H.; Case, D. A. J Comput Chem 2004, 25(2), 238-250.
88. Bao, D.; Bian, H.; Xu, D.; Zhao, C.; Jin, Q.; Zhu, M.; Tao, T.; Cai, J. Int J Pept Res Ther 2018, 1-7.
89. Weis, A.; Katebzadeh, K.; Söderhjelm, P.; Nilsson, I.; Ryde, U. J Med Chem 2006, 49(22), 6596-6606.
90. Hou, T.; Wang, J.; Li, Y.; Wang, W. J Chem Inf Model 2010, 51(1), 69-82.
91. Jastrzebska, B.; Chen, Y.; Orban, T.; Jin, H.; Hofmann, L.; Palczewski, K. J Biol Chem 2015, 290(42), 25728-25744.
92. Wimley, W. C.; White, S. H. Biochemistry 2000, 39(15), 4432-4442.
93. Hebert, T. E.; Moffett, S.; Morello, J.-P.; Loisel, T. P.; Bichet, D. G.; Barret, C.; Bouvier, M. J Biol Chem 1996, 271(27), 16384-16392.
94. Stone, T. A.; Deber, C. M. Biochim Biophys Acta Biomembr 2017, 1859(4), 577-585.
95. Ferré, S. Trends Pharmacol Sci 2015, 36(3), 145-152.
96. Singer, S. J.; Nicolson, G. L. Science 1972, 175(4023), 720-731.
97. Pike, L. J. J Lipid Res 2009, 50(Supplement), S323-S328.
98. Cooper, D. M.; Crossthwaite, A. J. Trends Pharmacol Sci 2006, 27(8), 426-431.
99. Chen, L.; Novicky, L.; Merzlyakov, M.; Hristov, T.; Hristova, K. J Am Chem Soc 2010, 132(10), 3628-3635.
100. Mineev, K. S.; Lesovoy, D. M.; Usmanova, D. R.; Goncharuk, S. A.; Shulepko, M. A.; Lyukmanova, E. N.; Kirpichnikov, M. P.; Bocharov, E. V.; Arseniev, A. S. Biochim Biophys Acta Biomembr 2014, 1838(1), 164-172.
101. Huang, D.; Qi, Y.; Song, J.; Zhang, J. Z. J Comput Chem 2019, 40(9), 1045-1056.
102. Wang, E.; Sun, H.; Wang, J.; Wang, Z.; Liu, H.; Zhang, J. Z.; Hou, T. Chem Rev 2019, 119(16), 9478-9508.
103. Bhatia, S.; Diedrich, D.; Frieg, B.; Ahlert, H.; Stein, S.; Bopp, B.; Lang, F.; Zang, T.; Kroger, T.; Ernst, T.; Kogler, G.; Krieg, A.; Ludeke, S.; Kunkel, H.; Rodrigues Moita, A. J.; Kassack, M. U.; Marquardt, V.; Opitz, F. V.; Oldenburg, M.; Remke, M.; Babor, F.; Grez, M.; Hochhaus, A.; Borkhardt, A.; Groth, G.; Nagel-Steger, L.; Jose, J.; Kurz, T.; Gohlke, H.; Hansen, F. K.; Hauer, J. Blood 2018, 132(3), 307-320.
104. Arkin, M. R.; Wells, J. A. Nat Rev Drug Discov 2004, 3(4), 301.
105. Clackson, T.; Wells, J. A. Science 1995, 267(5196), 383-386.
106. Popowicz, G. M.; Czarna, A.; Wolf, S.; Wang, K.; Wang, W.; Dömling, A.; Holak, T. A. Cell cycle 2010, 9(6), 1104-1111.
107. Harikumar, K. G.; Dong, M.; Cheng, Z.; Pinon, D. I.; Lybrand, T. P.; Miller, L. J. Biochemistry 2006, 45(49), 14706-14716.

108. Borroto-Escuela, D. O.; Rodriguez, D.; Romero-Fernandez, W.; Kapla, J.; Jaiteh, M.; Ranganathan, A.; Lazarova, T.; Fuxe, K.; Carlsson, J. Front Pharmacol 2018, 9.